Available online at www.sciencedirect.com
ScienceDirect
Journal of the European Ceramic Society 26 (2006) 3525–3530
www.elsevier.com/locate/jeurceramsoc

Fabrication of pore-gradient Al_2O_3–ZrO_2 sintered bodies by fibrous monolithic process

Byong-Taek Lee [a,*], In Cheol Kang [a], Asit Kumar Gain [a], Ki-Ho Kim [a], Ho-Yeon Song [b]

[a] *School of Advanced Materials Engineering, Kongju National University, 182, Shinkwan-dong, Kongju City, Chungnam 314-701, South Korea*
[b] *Department of Microbiology, School of Medicine, Soonchunhyang University, 366-1, Ssangyoung-dong, Cheonan-city, Chungnam 330-090, South Korea*

Received 14 September 2005; received in revised form 12 December 2005; accepted 17 December 2005
Available online 23 February 2006

Abstract

Functionally pore-gradient Al_2O_3–ZrO_2 composites where the porosity is dependent on the extrusion ratio and number of shell layer were fabricated by a fibrous monolithic process. The size and volume fraction of the pores were controlled by different numbers of shell layers, which contained various sizes and a different volume percentage of the pore-forming agent. In the pore-gradient, Al_2O_3–ZrO_2 bodies having a dense core part, some defects such as cracks, swelling and delamination occurred during the sintering process due to the low extrusion ratio. However, these defects were completely removed as the extrusion ratio increased, and the shell layers as well as the core part had a continuously porous structure. In the shell part, various sizes of pores from 70 to 250 μm in diameter were observed.

Keyword: Pore-gradient; Microstructure; Composites; Al_2O_3–ZrO_2

1. Introduction

Al_2O_3 and ZrO_2 ceramics have received a lot of attention as biomaterials from many researchers due to their advantages such as excellent biocompatibility, excellent chemical stability and good corrosion resistance as well as outstanding mechanical properties.[1–3] However, the dense Al_2O_3 and ZrO_2 bodies showed low osteoconductivity, which has restricted their application as implant materials. To improve osteoconductivity, porous Al_2O_3 and ZrO_2 bodies are required so that cancellous bone can be easily grown on the artificial implants. Thus, many researchers have focused on the formation of porous materials and made a rough pore surface. In general, the suitable pore size for implant materials is about 100–150 μm,[4] 140–160 μm[5] and 200–1000 μm.[6]

Several fabrication processes such as ceramic/carbon mixture,[7] tape casting[8] and centrifugal molding technique[9] have been used to make pore-gradient materials, but, these processes do not control the pore size and pore-gradient rate as well as the modification of the uniform porous core structure. Recently, an innovative fibrous monolithic process was adapted to manufacture highly toughened ceramic bodies as well as to control the pore size and shape.[10–12]

In this work, this new approach was used to fabricate pore-gradient Al_2O_3–ZrO_2 ceramic bodies using the fibrous monolithic process. The various parameters such as extrusion ratio, pore-gradient rate, pore size and microstructure were changed to set up optimum conditions for fabrication of pore-gradient Al_2O_3–ZrO_2 bodies. To evaluate their mechanical behavior, the microstructure and the tendency to phase transformation depending on the fabrication procedure, three-point bending tester, BSE-SEM, optical microscopy and XRD techniques were used.

2. Experimental procedure

Al_2O_3 (about 0.3 μm, AKP-50, Sumitomo, Japan), ZrO_2 (about 80 nm, *m*-ZrO_2, Tosho, Japan) and carbon (50–200 μm, SMC, Korea) powders were used as starting materials. Ethylene vinyl acetate (EVA) (ELVAX 210 and 250, Dupont, USA) and stearic acid ($CH_3(CH_2)_{16}COOH$, Daejung Chemicals &Metals Co., Korea) were added as binder and lubricant, respectively. Different volume ratio (25:75, 40:60, 60:40 and 80:20 vol.%) of (75 vol.% Al_2O_3–25 vol.% ZrO_2) and car-

* Corresponding author. Tel.: +82 41 850 8677; fax: +82 41 858 2939.
E-mail address: lbt@kongju.ac.kr (B.-T. Lee).

0955-2219/$ – see front matter © 2006 Elsevier Ltd. All rights reserved.
doi:10.1016/j.jeurceramsoc.2005.12.017

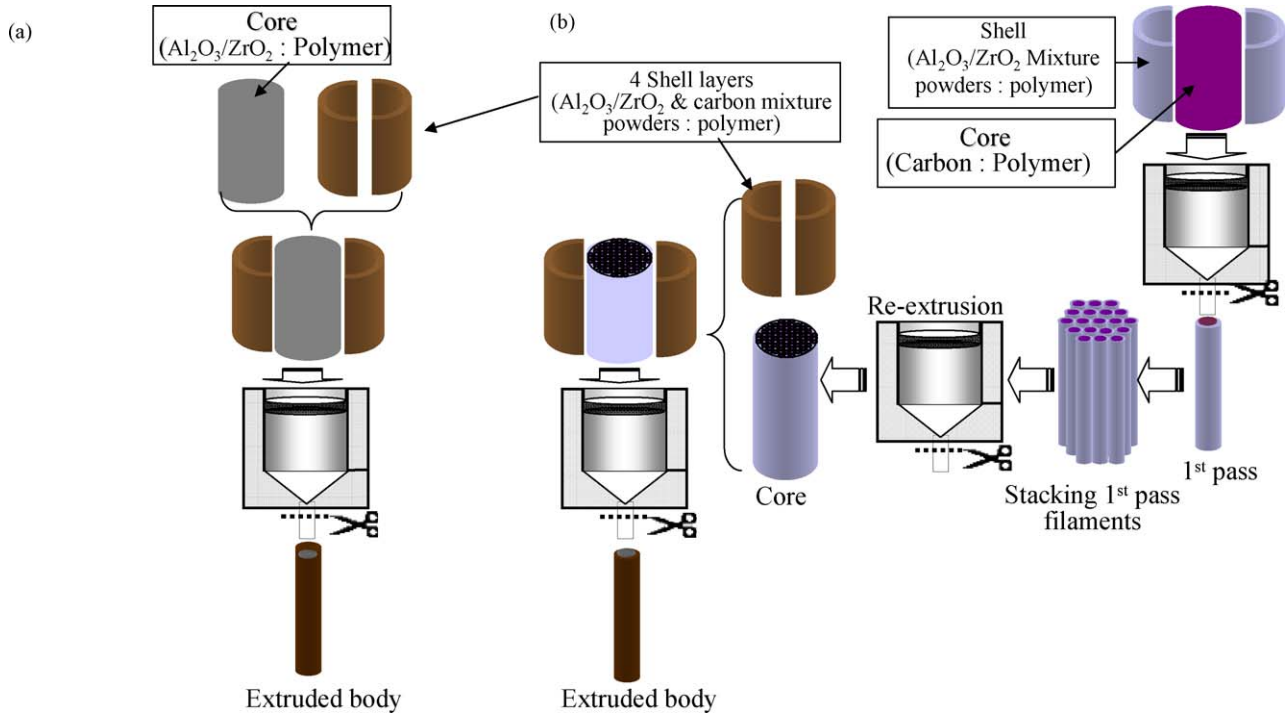

Fig. 1. Schematic diagram of fabrication process of pore-gradient Al_2O_3–ZrO_2 sintered body: (a) dense and (b) continuously porous core.

bon powders were homogeneously mixed in ethanol by a ball mill process using Al_2O_3 balls as milling media. After mixing, each composition was dried on a hotplate while stirring. The different volume ratio of ball milled mixture of powders (Al_2O_3–ZrO_2/carbon)/EVA/stearic acid (volume fraction 60:30:10) was separately mixed using a shear mixer (Shina Platec Co., Korea) at 120 °C for 1 h. Using these four kinds of shear-mixed materials, 2 mm thick shell layer of each composition was made by warm pressing. To make the dense core pore-gradient bodies, the rod type core, 21 mm in diameter, was made by extrusion process using the Al_2O_3–ZrO_2/EVA mixture. These four-shell layers and core were assembled together and extruded into filament at 120 °C with different extrusion ratios (2.5:1, 11.9:1 and 19.3:1) as shown in Fig. 1(a).

On the other hand, to make the continuously porous core structure, at first, Al_2O_3–ZrO_2/EVA mixture was used to make a 4 mm thick shell layer by warm pressing and a rod type core was made by the extrusion process using only pore forming agent (carbon)/EVA mixture. This shell and core were assembled together and extruded in a heated die to make the 1st passed filaments having 3.5 mm in diameter. The 1st passed filaments were cut and reloaded in a steel die and extruded to make a 21 mm diameter rod type core. Then, the before making four shell layers and this core were assembled together and extruded into filament at 120 °C with extrusion ratio (19.3:1) as shown in Fig. 1(b).

To remove the EVA binder and pore-forming agent (carbon) in both samples, the 1st and 2nd burning-out processes were carried out at 700 and 1000 °C for 2 h under N_2 atmosphere and air, respectively. Finally, the pressureless sintering was carried out at 1550 °C for 2 h in air atmosphere. Microstructures were examined using optical photography, a back-scattered electron scanning electron microscope (BSE-SEM, JEOL-JSM 5410) and transmission electron microscopy (TEM, JEM-2010, JEOL) techniques. The crystal phases were analyzed by X-ray diffraction (XRD, D/MAX-250, Rigaku, Japan) using Cu Kα of 0.1542 nm. To measure the fracture strength, a three-point bending strength test was carried out using UTM (R&B Co., Korea).

3. Results and discussion

Fig. 2 shows photographs of sintered Al_2O_3–ZrO_2 bodies depending on the number of shell layers and the extrusion ratio. In Fig. 2(a), the sample consisted of two-shell layers and was extruded with a low extrusion ratio (2.5:1). After sintering, shell delamination occurred as indicated by an arrowhead, due to the low extrusion ratio. In Fig. 2(b), the sample consisted of four shell layers and was extruded with a ratio of 11.9:1. Some delamination phenomenon, as indicated with an arrowhead, was observed, also due to the low extrusion ratio. On the other hand, using the same number of shell layers and increasing the extrusion ratio (19.3:1), bulk defects, which appeared in Fig. 2(a) and (b), were not observed. However, in Fig. 2(d), the core structure was modified with the continuously porous structure. The pore size of the continuously porous core region was about 255 μm in diameter.

Fig. 3 shows the XRD patterns of (a) raw Al_2O_3 and (b) *m*-ZrO_2 powder, (c) after the 1st burning-out, (d) after the 2nd burning-out and (e) pore-gradient Al_2O_3–ZrO_2 sintered bodies at 1550 °C. After the 1st burn-out, carbon (pore-forming agent) peaks were detected as well as Al_2O_3 and *m*-ZrO_2 phases. How-

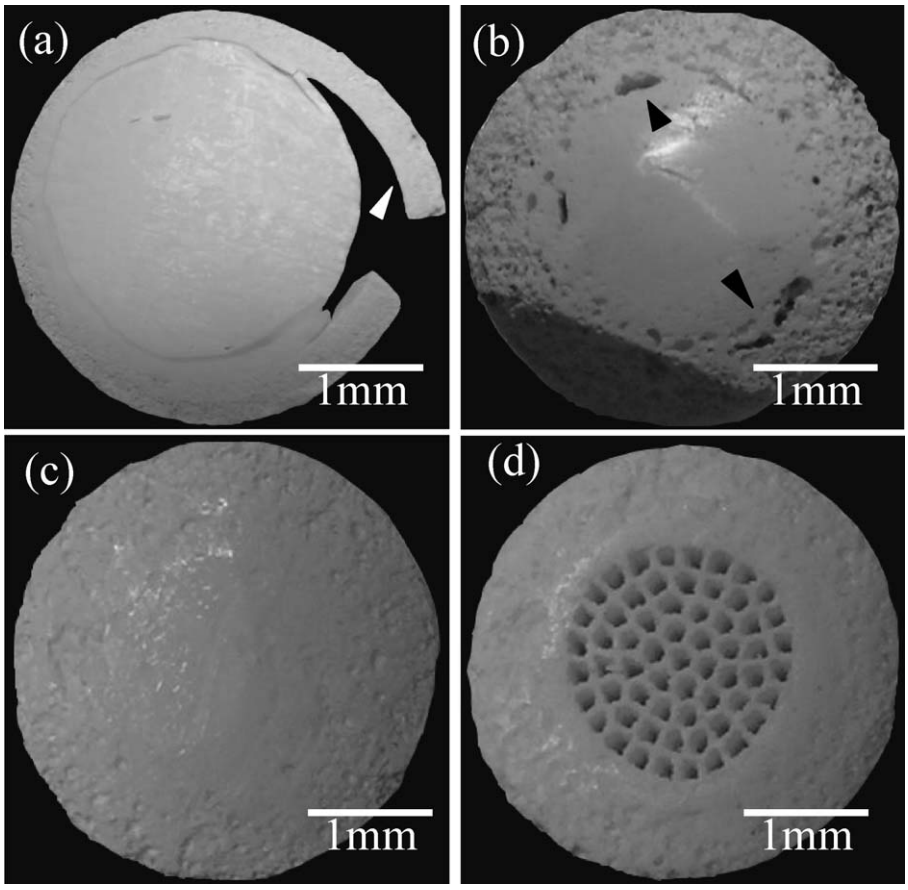

Fig. 2. Photographs of pore-gradient Al_2O_3–ZrO_2 sintered bodies depending on the number of layers and extrusion ratio: (a) two layers: 2.5:1, (b) four layers: 11.9:1, (c) four layers: 19.3:1 and (d) four layers: 19.3:1.

ever, after the 2nd burn-out, the carbon was not detected as shown in Fig. 3(d). After sintering, the pore-gradient bodies were composed of Al_2O_3 and *m*-ZrO_2 phases as shown in Fig. 3(e).

Fig. 4 shows SEM micrographs of (a) before and (b) after sintering of pore-gradient Al_2O_3–ZrO_2 bodies having a dense core structure and two shell layers. The inner shell of the extruded body contained 40 vol.% carbon while the outer shell contained 70 vol.% carbon. After sintering, different sizes of pores about 70–100 μm in diameter were produced in the inner shell while the pore size of the outer shell was about 150–250 μm in diameter (b). Fig. 4(c) and (d) are partially enlarged images of outer shell and shell boundary regions of Fig. 4(b). As shown in Fig. 4(c), the outer shell has various sizes of pore sizes, which offers the advantages of good adherence and growth of cells. From observation of the cross-sectional SEM micrograph at the interface between the layers in Fig. 4(d), no defects such as swelling or delamination in the boundary were found. Moreover, each layer shows a uniform pore size, respectively. However, some cracks were found as shown in Fig. 4(b) as indicated with arrowheads between the dense core and porous shell region.

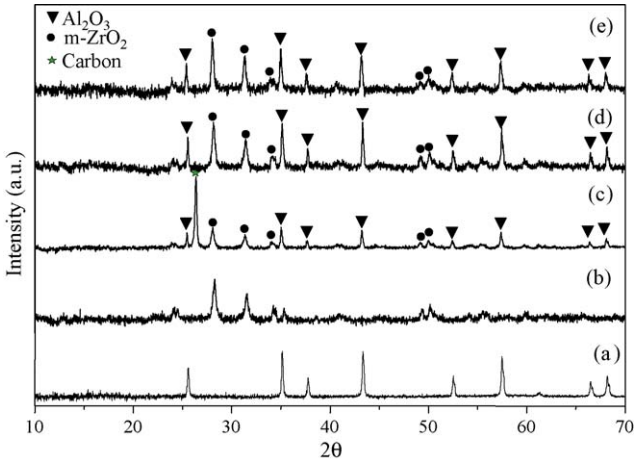

Fig. 3. XRD profiles of (a) raw Al_2O_3 powder, (b) raw *m*-ZrO_2 powder, (c) after 1st burn-out, (d) after 2nd burn-out and (e) sintered at 1550 °C of extruded Al_2O_3–ZrO_2 bodies.

Fig. 5 shows BSE–SEM images of (a and b) longitudinal and (c and d) cross-sectional directions of pore-gradient Al_2O_3–ZrO_2 bodies (a and c) before and (b and d) after sintering, respectively. As shown in Fig. 5(a) and (c), the pore-forming agent which appeared with a dark contrast, as indicated with arrowheads, was homogeneously and gradient dispersed in the Al_2O_3–ZrO_2 matrix. However, after the burning-out and sintering process, the pore-forming agent was removed and formed many pores as indicated with arrowheads in Fig. 5(b and d). After sintering, bulk defects such as cracks, delamination or swelling

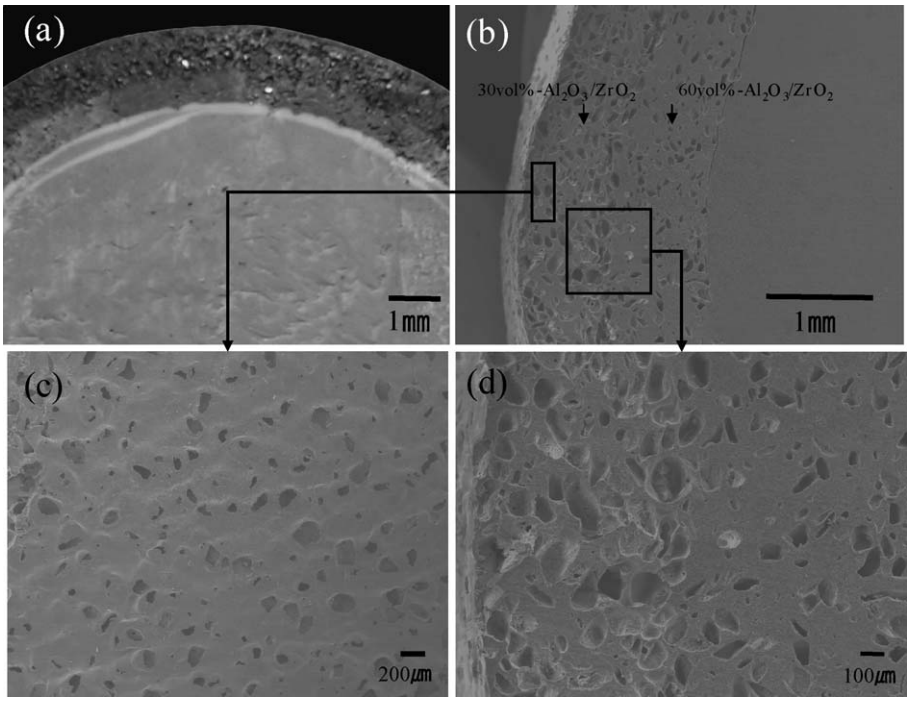

Fig. 4. SEM micrographs of pore-gradient Al_2O_3–ZrO_2 bodies (different pore size): (a) before and (b) after sintering. (c) Outer shell and (d) interface of shell layers.

were not found between the pore-gradient regions, but some cracks were observed in the dense core region. It was confirmed that the reason cracks were created was derived from thermal strain due to the different shrinkage between the dense core and porous shell region.

Fig. 6 shows the other pore-gradient microstructure of Al_2O_3–ZrO_2 bodies, which consist of a continuously porous core structure. Fig. 6(a) and (c) show BSE–SEM images of longitudinal and cross-sectional direction of pore-gradient Al_2O_3–ZrO_2 extruded bodies, respectively. Before sintering, in the core part, the pore forming agent (carbon) and EVA having 255 μm in diameter were homogeneously distributed as indicated with an arrowhead (c). After the burning-out and sintering process, the EVA binder and pore-forming agent (carbon) were

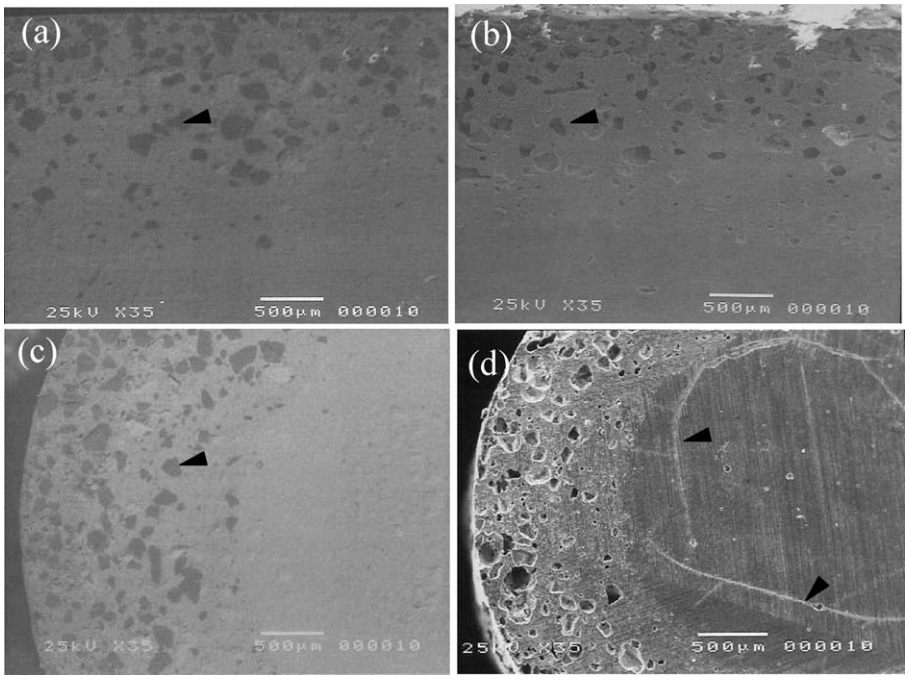

Fig. 5. BSE–SEM micrographs of pore-gradient Al_2O_3–ZrO_2 bodies (same pore size and dense core structure): (a and b) longitudinal and (c and d) cross-sectional direction and (a and c) before and (b and d) after sintering.

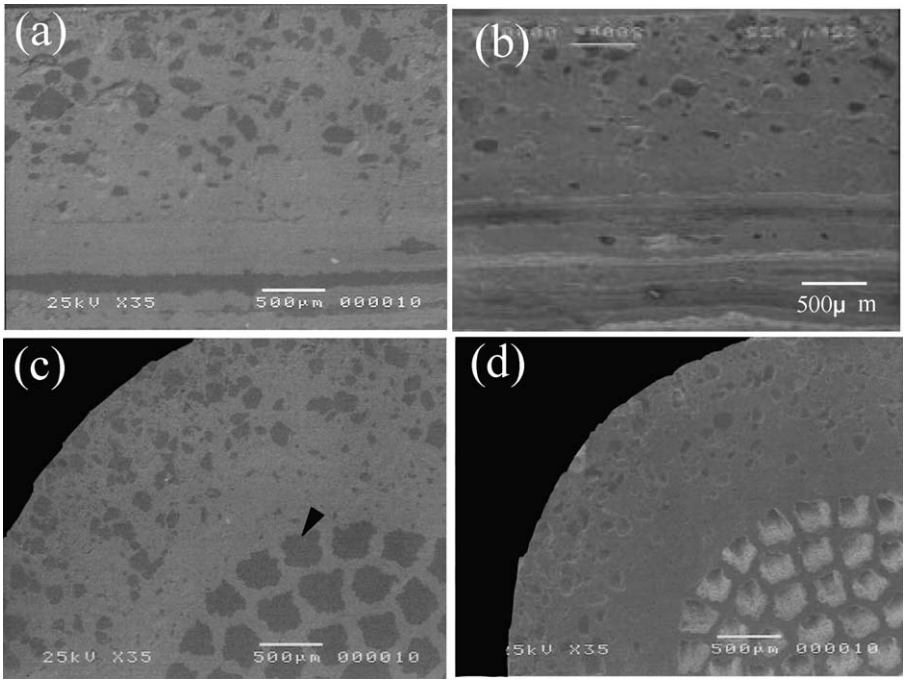

Fig. 6. BSE–SEM micrographs of Al_2O_3–ZrO_2 pore-gradient bodies (same pore size and porous core structure): (a and b) longitudinal and (c and d) cross-sectional direction and (a and c) before and (b and d) after sintering.

perfectly removed and formed continuous pores in the core part, but in the shell part, pores were present gradiently as shown in Fig. 6(d). However, in this case, bulk defects were not found between the shell layers or in the continuously porous core part.

Fig. 7(a) shows a TEM image (a) of the pore-gradient Al_2O_3–ZrO_2 bodies. In the TEM micrograph (a), the Al_2O_3 grains showed a bright contrast about 700 nm in diameter while *m*-ZrO_2 grains were seen with a dark contrast about 250 nm in diameter. Most of the *m*-ZrO_2 phases were located at the grain boundaries. However, in the Al_2O_3 grains, a few *t*-ZrO_2 particles less than 150 nm in diameter were clearly observed as indicated by an arrowhead (a). An HRTEM micrograph (b) was taken from an *m*-ZrO_2 grain, which is marked b in Fig. 7(a). In the *m*-ZrO_2 grain, many twin boundaries were clearly observed as indicated with arrowheads (b). In general, these types of twins were formed to dissipate a shear stress, which was generated by a phase transformation during the sintering process.

Fig. 8 shows the load–distance curves of pore-gradient Al_2O_3–ZrO_2 bodies having (a) dense core and (b) porous core structures. At the initial stage, about 0.2 mm in distance, the load was increased about 7 kg and dramatically dropped in both samples, due to the fracture of the porous shell. But, in the case of the pore-gradient Al_2O_3–ZrO_2 bodies having a dense core, the load

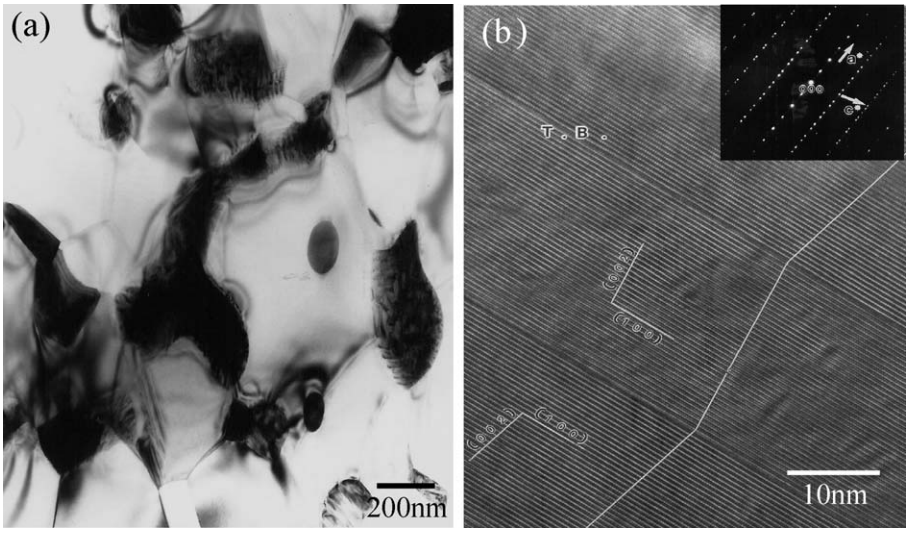

Fig. 7. TEM (a) and HRTEM (b) micrographs of pore frame region of pore-gradient Al_2O_3–ZrO_2 bodies.

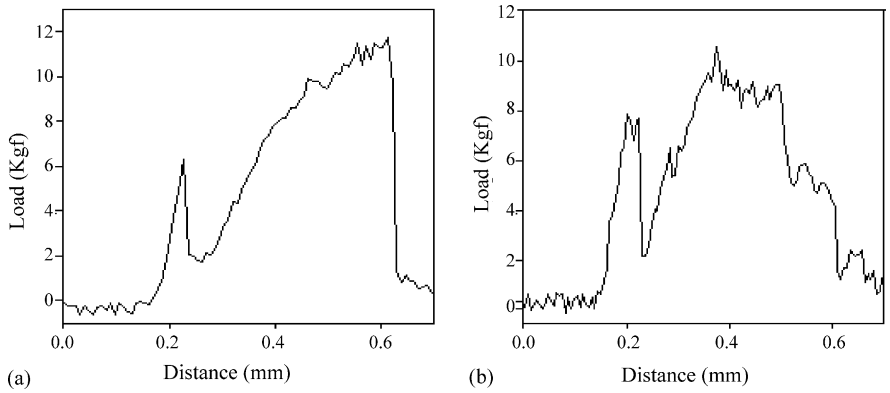

Fig. 8. Load–distance curves of Al_2O_3–ZrO_2 pore-gradient bodies: (a) dense core and (b) porous core.

was increased up to 11 kg as the distance increased from 0.25 to 0.55 mm and dramatically dropped due to the fracture of the dense core. The existence of cracks obtained in Fig. 5(d) may be promoted as the typical catastrophic failure. However, the pore-gradient Al_2O_3–ZrO_2 bodies having a porous core showed a different behavior; i.e., the load fluctuated before the main fracture due to the continuously porous structure as shown in Fig. 6(d). In general, the common ceramics showed a brittle fracture; thus, the load–distance curve increased linearly and dropped dramatically after the fracture. However, the pore-gradient Al_2O_3–ZrO_2 bodies showed semi-brittle fracture behavior, which appears in fibrous monolithic composites. The maximum values of bending strength of pore-gradient Al_2O_3–ZrO_2 bodies having a dense core and porous core microstructure were about 219.7 and 195.5 MPa, respectively. From our previous work, the values of bending strength strongly depended on porosity and pore size. In the continuously porous Al_2O_3 bodies having 63% relative density and 150 μm in diameter pore size, the bending strength value was about 90 MPa.[13]

4. Conclusions

Pore-gradient Al_2O_3–ZrO_2 sintered bodies were successfully fabricated using the fibrous monolithic process. The pore-gradient microstructure was easily controlled depending on the pore size and porosity, using the various sizes of carbon powder and changing the volume fraction of pore-agent. In pore-gradient bodies having a porous core structure, no bulk defects such as cracks and shrinkage cavities were found due to the reduction of the thermal strain by the formation of continuously porous core structure.

The load–distance curves of pore-gradient Al_2O_3–ZrO_2 bodies showed some different behavior, which appeared with that of common ceramics due to microstructure control, especially pore-gradient and porous core structure.

Acknowledgement

This work was supported by NRL research program of the Korean Ministry of Science and Technology.

References

1. Li, W. and Gao, L., Fabrication of HAp–ZrO_2 (3Y) nano-composite by SPS. *Biomaterials*, 2003, **24**, 937–940.
2. Jordan, D. R., Online clinical commun. for ophthalmologists (TM) – http://www.occojournal.com/. *Forum*, 2001, **31**.
3. Willmann, G., Fruh, H. J. and Pfaff, H. G., Wear characteristics of sliding pairs of ZrO_2(Y-TZP) for hip endoprostheses. *Biomaterials*, 1996, **17**, 2157–2162.
4. Hing, K. A., Best, S. M. and Bonfield, W., Characteristic of porous hyroxyapaptite. *J. Mater. Sci. Mater. Med.*, 1999, **10**, 135–145.
5. Hench, L. L., Bioceramics. *J. Am. Ceram. Soc.*, 1998, **81**, 1705–1728.
6. Chiroff, R. T., White, E. W., Webber, J. N. and Roy, D. M., Tissue ingrowth of replamineform implants. *J. Biomed. Mater. Res. Symp.*, 1975, **6**, 29–45.
7. Maca, K., Dobsak, P. and Boccaccini, A. R., Fabrication of graded porous ceramics using alumina–carbon powder mixtures. *Ceram. Int.*, 2001, **27**, 577–584.
8. Werner, J., Krcmar, B. L., Friess, W. and Greil, P., Mechanical properties and in vitro cell compatibility of hydroxyapatite ceramics with graded pore structure. *Biomaterials*, 2002, **23**, 4285–4294.
9. Chen, C. H., Takita, K., Honda, S. and Awaji, J., Fracture behavior of cylindrical porous alumina with pore gradient. *J. Eur. Ceram. Soc.*, 2005, **25**, 385–391.
10. Kaya, C., Butler, E. G. and Lewis, M. H., Co-extrusion of Al_2O_3/ZrO_2 biphase high temperature ceramics with fine scale aligned microstructures. *J. Eur. Ceram. Soc.*, 2003, **23**, 935–942.
11. Lienard, S. Y., Kovar, D., Moon, R. J., Bowman, K. J. and Halloran, J. W., Texture development in Si_3N_4/BN fibrous monolithic ceramics. *J. Mater. Sci.*, 2000, **35**, 3365–3371.
12. Kim, T. S., Kang, I. C., Goto, T. and Lee, B. T., Fabrication of continuously porous alumina body by fibrous monolithic and sintering process. *Mater. Trans.*, 2003, **44**, 1851–1856.
13. Lee, B. T., Kang, I. C., Cho, S. H. and Song, H. Y., Fabrication of continuously oriented porous Al_2O_3 body and its in-vitro study. *J. Am. Ceram. Soc.*, 2005, **88**, 2262–2266.